DOI: 10.15669/pnst.7.381

Progress in Nuclear Science and Technology
Volume 7 (2025) pp. 381-387

ARTICLE

Study of proton distribution in the backing material of accelerator neutron source solid target by ERDA analytical techniques

Hong-Fu Liu [a], Naoto Hagura [a, *], Tomohiro Kobayashi [b] and Jun Kawarabayashi [a]

[a] *Tokyo City University, 1-28-1 Tamazutsumi, Setagaya, Tokyo 158-8557, Japan;*
[b] *RIKEN, 2-1 Hirosawa, Wako, Saitama 351-0198, Japan*

Compact accelerator-driven neutron sources have expanded the range of neutron beam applications and promise a wide range of industrial applications. The development of long-life target structures will facilitate the widespread use of compact accelerator-driven neutron sources. The backing material in the target structure acts as a stopping region for the high-energy proton beam, and the protons accumulated in the backing material can diffuse into the connection between the neutron generation film and the backing material, leading to the breakdown of the lithium or beryllium film, thus affecting the target lifetime. Therefore, it is necessary to understand the proton distribution in the backing material when designing the target. In this study, we aim to develop practical solid targets for compact accelerator-driven neutron sources, discuss the proton distribution in the backing material after proton implantation, and present fundamental data for the design of the backing material. Hydrogen ion implantation was performed using a Penning ionization gauge (PIG) negative ion source at the Atomic Energy Research Laboratory, Tokyo City University. The energy of the implanted H^- ion was 20 keV, and the hydrogen distribution of the irradiated samples was analyzed using elastic recoil detection analysis (ERDA) of the RIKEN Pelletron tandem accelerator. The ERDA spectra were compared with those calculated using the Stopping and Range of Ions in Matter (SRIM) and SIMNRA codes.

Keywords: accelerator-driven neutron source; PIG negative ion source; SRIM; ERDA; hydrogen implantation

1. Introduction

Compact accelerator-driven neutron sources are expected to expand the range of neutron beams and are widely used in industrial applications. The $^{7}Li(p,n)^{7}Be$ reaction gives relatively high neutron yields even at low-energy protons [1]. Neutrons generated at low-energy protons are easily shielded and are suitable for compact accelerator-driven neutron sources. The typical current of proton beams used in compact accelerator-driven neutron sources is typically between tens of microamperes (μA) and several milliamperes (mA). The RIKEN accelerator-driven neutron system II (RANS-II) successfully generated neutrons in 2019 and was proven suitable for nondestructive inspections. The main components of RANS-II include an electron-cyclotron-resonance (ECR) ion source, a 2.5 MeV radio frequency quadrupole (RFQ), a solid-state amplifier, and a solid lithium neutron generation film crimped on a copper backing material.

The proton beam energy, current, and power of the RANS-II are 2.49 MeV, 100 μA, and 0.25 kW, respectively, as shown in **Figure 1** [2]. To prevent the solid lithium target from evaporating at high temperatures, the target is cooled using water circulation. The target structure of the RANS-II at this stage is shown in **Figure 2**. The lithium film is fixed onto the copper backing material by pressure bonding, and the lithium film surface is coated with chromium nitride (CrN) to prevent oxidation of the lithium due to air contact during the exchange of the neutron generation target.

At this stage, the design of the solid target backing material for the RANS-II is only considered from the perspective of heat conduction, so copper with excellent thermal conductivity is used as the backing material. To prevent breakage of the lithium film caused by hydrogen aggregation when the protons stop in the lithium film, the appropriate thickness of the lithium film is discussed using the Stopping and Range of Ions in Matter (SRIM) code. Based on the SRIM results (**Figure 3(a)**), the stopping depth of a 2.49 MeV proton beam at the lithium metal layer is 236 μm. To prevent the 2.49 MeV proton stopping at the lithium layer and causing hydrogen aggregation to break down the lithium film structure, making the proton beam pass through the lithium film is necessary. **Figure 3(b)** shows the proton distribution of the solid lithium target at this stage obtained from the SRIM calculations. Based on the SRIM calculations, the

*Corresponding author. E-mail: nhagura@tcu.ac.jp

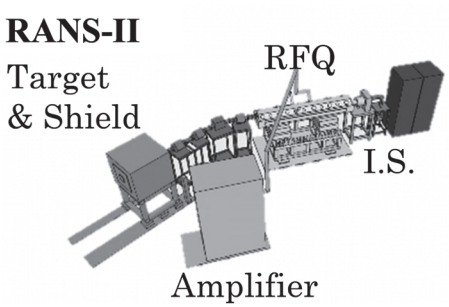

	RANS-II
Particle	Proton
Energy	2.49 MeV
Current	100 μA
Reaction	^{7}Li(p, n)^{7}Be
Accelerator	RFQ
Weight(Accelerator)	3 t
Weight(Target&Shield)	< 0.7 t
Length	< 5 m

Figure 1. Configuration and parameters of the RANS-II.

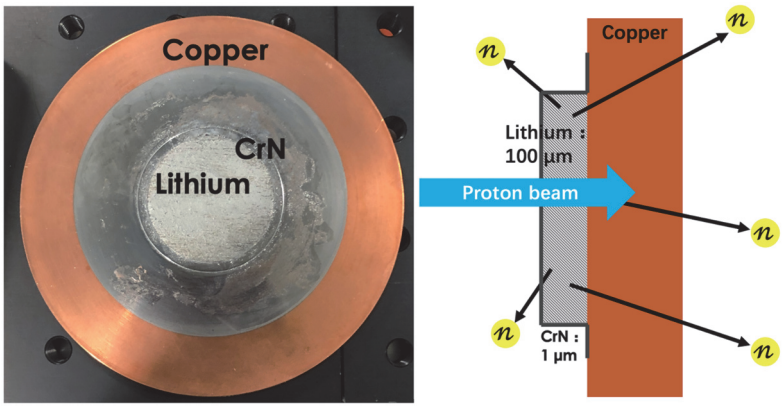

Figure 2. Structure of the RANS-II solid neutron generation target.

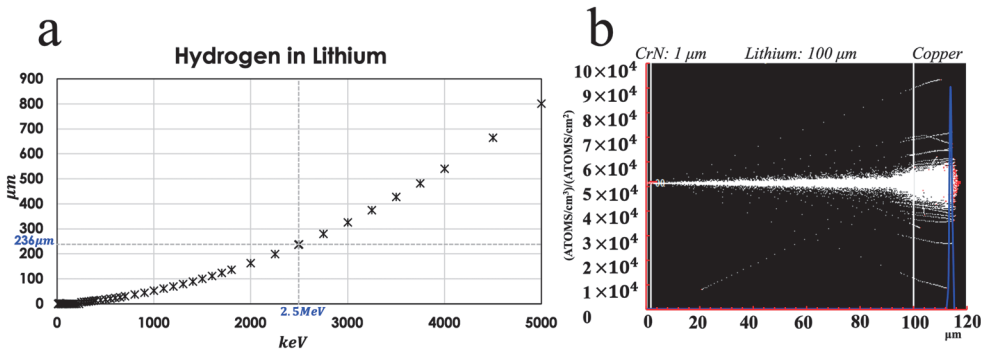

Figure 3. (a) Stopping range of hydrogen in lithium obtained from the SRIM calculations, (b) Calculation of the 2.49 MeV proton beam stopping range in the RANS-II solid target.

2.49 MeV proton beam passes through the 1 μm thick CrN and 100 μm thick lithium target, stopping in copper with a stopping depth of about 16 μm.

2. Purpose

In designing the backing material for solid neutron generation targets and to prevent blistering due to proton storage between the neutron generation film and backing material, Yamagata et al. [3] simulated the behavior of hydrogen movement in the backing material during proton implantation using finite element software and SRIM calculations. The simulations were performed for a RANS solid beryllium target based on a hydrogen diffusion perspective. The simulation results showed that the maximum hydrogen concentration was well below the embrittlement limit for vanadium, niobium, tantalum, and palladium. However, the low hydrogen diffusion capacity of aluminum and copper led to hydrogen concentrations up to 10 times higher than the embrittlement limit, indicating that the use of copper or aluminum backing materials could cause blistering problems within a short period, resulting in breakage of the target structure. For a backing material with high hydrogen diffusion ability, the protons stopping near the surface of the backing material may diffuse into the junction between the backing material and neutron generation layer, resulting in hydrogen accumulation and rupture of the target structure.

Concerned that this would be a problem related to blistering, therefore an experimental system is investigated to analyze the distribution and diffusion behavior of protons implanted in the backing material. Proton implantation research methods are now widely used in nuclear fusion, and many studies have used low-energy proton beams to irradiate samples to investigate the effect of residual hydrogen on the material properties when the plasma walls are irradiated by protons [4]. Nevertheless, no relevant research has been conducted on targets of accelerator-driven neutron sources irradiated with low-energy proton beams.

Understanding the behavior of protons in the backing material is essential for developing long-life solid targets for compact accelerator-driven neutron sources. To clarify the behavior of protons near the interface, we performed low-energy ion irradiation on the backing materials.

3. Method

The sample materials were irradiated with low-energy protons, and the proton distribution and content were examined using the ion beam analysis method.

3.1. Determination of irradiated samples

To prevent blistering problems due to hydrogen diffusion, hydrogen absorbing alloys are expected to replace the existing copper backing material considering the hydrogen absorptive capacity of metals. Therefore, to select the irradiated sample materials for the background metals, we considered the following aspects: (1) metal hydrogenation reaction, (2) neutron radiation, (3) metal compatibility, and (4) thermal conductivity. The primary commercially available hydrated metals for hydrogenation reactions are rare earth, titanium, and magnesium alloys. Magnesium alloys need to be hydrogenated at 200°C, whereas rare earth alloys and titanium alloys can be hydrogenated at a pressure of less than 1 MPa and a temperature of less than 100°C [5]. In terms of the metal radioactivity associated with neutron absorption, radioactivity decay is fastest for magnesium alloys, followed by titanium alloys [6]. In terms of the connection between the lithium layer and backing material, taking into account the metal compatibility and bonding method, lithium and magnesium can form an alloy system, and the lithium and titanium layers can be connected using lithium–titanium compounds [7,8]. The thermal conductivities of magnesium alloys are superior to those of titanium alloys. Since the melting point of lithium in the RANS-II solid lithium target is 180.5 °C, titanium alloy was chosen as an alternative to the copper backing material in this study.

3.2. Low energy proton implantation

Two critical factors need to be considered in proton implantation: (1) implantation fluence and (2) energy of protons. In terms of the implantation proton energy, it takes a long time to achieve a high hydrogen concentration if the MeV proton beam is used for hydrogen implantation. In contrast, the keV proton beam can achieve a hydrogen concentration of several percent within a shorter period, and the keV proton beam is more conducive to observe the behavior of implanted hydrogen migration to the surface of the backing material.

In this study, we used the Penning ionization gauge (PIG, also known as cold cathode ionization gauge) negative ion source for hydrogen implantation at the Atomic Energy Research Laboratory, Tokyo City University. The extracted proton energy of the PIG negative ion source can be adjusted in the range of 0-25 keV, the implantation direction can be adjusted in the range of 0-180°, and the beam can be focused using an Einzel lens. A 20 keV proton beam was used to irradiate the samples vertically to obtain the highest irradiation dose at our facility. **Table 1** lists the conditions used for proton implantation using the PIG negative ion source. To prevent the surface bumpiness of samples from affecting the ion beam analysis results, the samples were polished to a mirror finish using a diamond abrasive, and the surface roughness was confirmed using a high-resolution scanner. In addition, all samples were placed in a dry environment at room temperature before irradiation.

The duration of irradiation were 1,000 and 600 min for the titanium and copper samples, respectively. The amount of implanted H^- was converted by the Faraday cup. The beam cross-section at a lens voltage of 11.9 kV was obtained using GAFchromic film and the beam current density per unit area was calculated using the current value and cross-sectional area. The sample area in this study was 10 mm × 15 mm, and thus, based on the calculation results, the number of H^- irradiated onto the samples was 8.9×10^{11} ions/s. Hence, the beam density was approximately 5.9×10^{11} ions/(s × cm^2) in the absence of apparent sputtering.

Table 1. Proton implantation conditions of the PIG negative ion source [9].

Hydrogen ion implantation conditions (Cold Cathode PIG Negative Ion Source)	
Plasma discharge voltage	830 V
Plasma discharge current	30 mA
Vacuum	7.5×10^{-3} Pa
Extraction voltage	20 kV
Beam convergence voltage	11.9 kV

3.3. Hydrogen distribution measurements

The microscopic existence state of protons in solids can be detected using nuclear magnetic resonance (NMR) and electron spin resonance (ESR), whereas the depth distribution of hydrogen can be measured using secondary ion mass spectrometry (SIMS) and other methods. Matsunami [10] discussed different hydrogen measurement methods, such as nuclear reactions, proton elastic scattering, forward scattering, and recoil particle detection. The

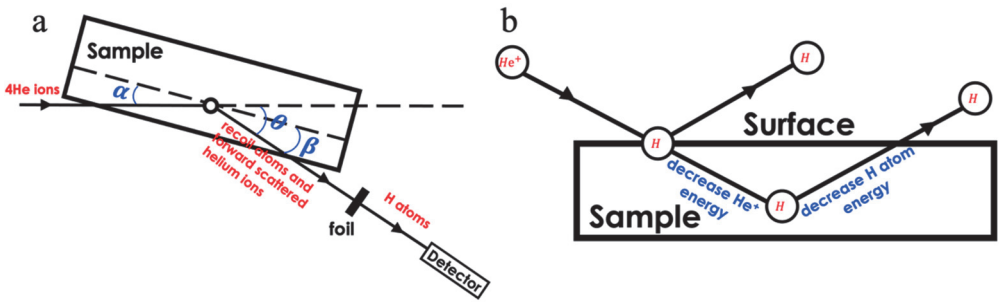

Figure 4. (a) Measurement system and (b) working principle of the ERDA method.

nuclear reaction method can achieve a resolution of 40 Å, whereas the forward scattering method has a detection sensitivity of 1 ppm. However, for these methods, the sample thickness needs to be extremely thin. The elastic recoil detection analysis (ERDA) of ^{4}He can measure the overall distribution of implanted protons within a short period and does not require excessive sample preparation. Therefore, in this study, the ERDA method was used to analyze the hydrogen distribution of the samples.

The measurement system and working principle of the ERDA method are shown in **Figure 4**. Rutherford backscattering spectrometry (RBS) irradiates helium ions in a direction almost perpendicular to the sample, the high-energy helium ions are passed onto the sample and measuring the energy distribution while a backscattered yield at a given angle. In contrast, the ERDA measurement system ejects hydrogen atoms from the sample by shooting ^{4}He ions into the sample at a shallow angle and uses a multichannel analyzer to measure the number and energy of the ejected hydrogen atoms. Similar to RBS, ERDA can perform depth analysis because the energy loss value suffered by the incident ^{4}He particles and the recoil H particles when traveling in the material can be accurately converted into the depth scale, and the number of H particles in the sample is reflected by the count rate of the detector.

The hydrogen distribution of the irradiated samples was determined using the ERDA beam line of the RIKEN Pelletron tandem accelerator. To obtain adequate results, the measured charge was set at 10 μC. The ERDA settings are tabulated in **Table 2**. To eliminate the effects of water and oil adsorbed on the surface, non-irradiated titanium and copper were also analyzed and subtracted as the background. The proton distribution of 20 keV protons implanted into the metal was calculated using the SRIM code and the ERDA spectra is simulated using the SIMNRA code based on the proton distribution calculation of SRIM [11]. And compare the differences between the simulated spectra and ERDA experimental spectra.

Table 2. ERDA measurement conditions.

ERDA setting parameters	
Incident ion	2275 keV He^{2+}
Helium beam spot area	2 mm × 8 mm
Charge amount for measurement	10 μC
Incidence angle (α)	15°
Measurement angle (θ)	30°
Detector active area	50 mm^2
Sample-detector distance	150 mm
Thickness of Al foil used as a stopper	14 μm

4. Results

The shape of the proton distribution for monoenergetic protons implanted into a metal sample approximates a Gaussian distribution. Also, since there was no significant asymmetry in obtained ERDA spectra, all experimental and simulation spectra were fitted with a Gaussian distribution model to facilitate comparison of the peak center position and full width at half maximum (FWHM) of the proton distribution.

The Monte Carlo code SRIM was used to calculate the hydrogen distributions of 20 keV hydrogen atoms in copper and titanium. Based on the results, the thicknesses of the copper and titanium samples were set at 240 and 300 nm, respectively, in the SIMNRA code. Assuming that all implanted protons were stably present in the samples, the hydrogen distributions of the titanium and copper samples are shown in **Figure 5**.

Based on the hydrogen distributions shown in Figure 5 and the ERDA experimental parameters, the systematic uncertainties in the experimental and simulation processes using the SIMNRA code are discussed. Adjust the relative parameters of ^{4}He ion incident angle α and detector setting angle β and compare the spectra' peak position and FWHM changes. The simulation results in **Figure 6** show that deviations in the ^{4}He incidence angle and detector setting angle during the ERDA experiments can partially affect the ERDA spectra. Therefore, careful adjustment is required when performing ERDA experiments. Furthermore, for the detector distance d the corresponding detector solid angle varies extremely slightly within a deviation of ±10 mm. Hence, it can be deduced that a slight deviation in the detector distance during the experiment only has a minor effect on the ERDA spectra.

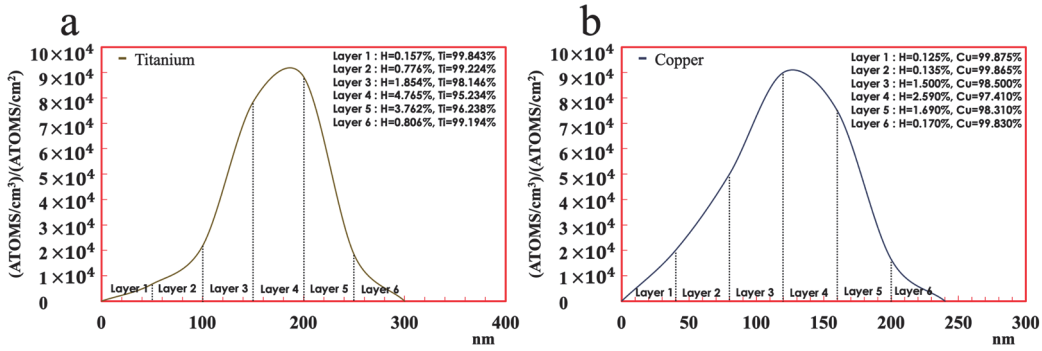

Figure 5. Hydrogen distributions of the (a) titanium and (b) copper samples based on SRIM calculations and current conversion.

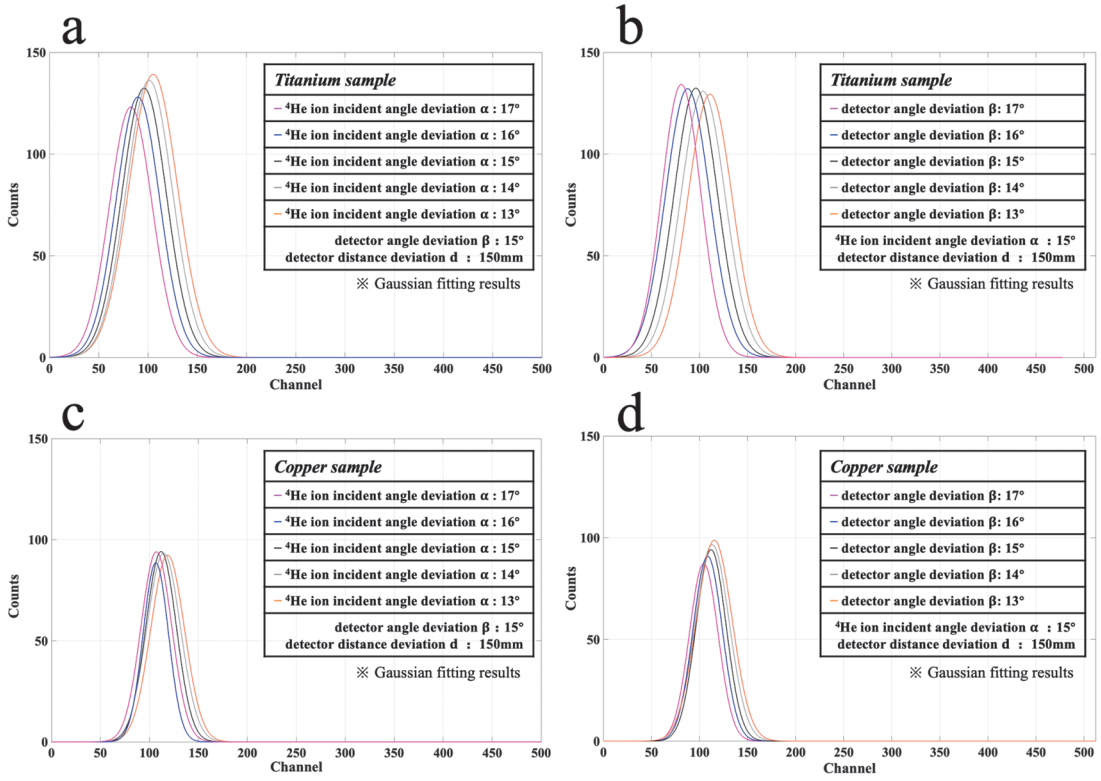

Figure 6. Calculation results of ERDA spectra under different parameters: (a) (c) detector setting angle and detector distance remained unchanged, ^{4}He ion incident angle was changed, (b) (d) ^{4}He ion incident angle and detector distance remained unchanged, detector setting angle was changed.

To eliminate the influence of adsorbed molecules on the samples on the ERDA measurement results, the ERDA measurements were performed on both hydrogen-implanted and nonhydrogen-implanted samples, and the ERDA spectra were obtained by calculating the difference in the hydrogen count rate. **Figure 7** shows the raw ERDA experimental data and the Gaussian distribution fitting results, and it is confirmed that the raw ERDA experimental data fit well with the Gaussian distribution. The peak positions and full width at half maximum of the spectra can be confirmed and can be compared with the simulation results by SIMNRA code. **Figure 8** summarizes the ERDA experimental spectra and the SIMNRA simulated spectra under the corresponding experimental parameters. Comparing the parameters of the Gaussian distribution of the spectra, the difference between the peak positions of the experimental and simulation spectra for the titanium sample was 2 channels with a 2.1% shift relative to the peak position of the simulation spectra, and for FWHM the difference between the simulation and experimental results for the titanium sample was 7 channels and the experimental results were 88.7% of the simulation results. For the copper sample, the difference between the peak position of the experimental and simulation spectra was 4 channels with a 3.6% shift relative to the peak position of the simulation spectra, and for FWHM the difference between the simulation and experimental results for the copper sample was 7 channels, the experimental results were 81.1% of the simulateion results. Comparing the peak positions and the full width

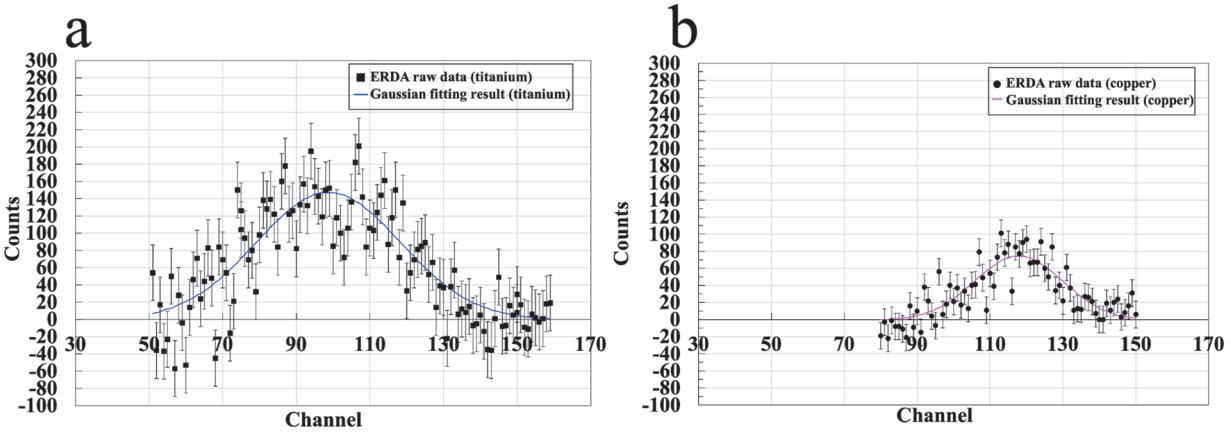

Figure 7. ERDA experimental raw data (with ±1 σ error bars) and Gaussian distribution fitting for the (a) titanium and (b) copper samples.

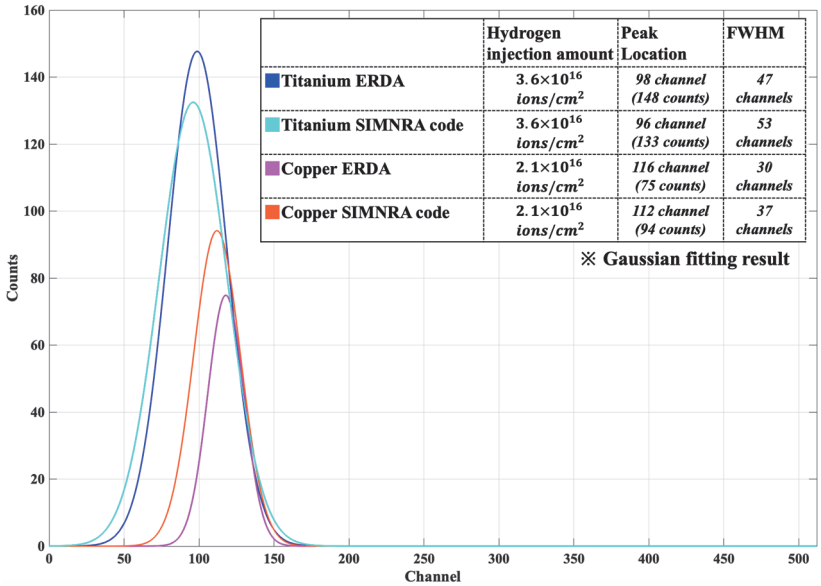

Figure 8. ERDA experimental spectra and SIMNRA simulation spectra for the titanium and copper samples.

at half maximum of the spectra, the experimental results and the simulation results were generally consistent, both simulation and experiment proceeded smoothly. Furthermore, based on the parameters of the spectra, it can be concluded that for a low-intensity proton beam with a beam density of 10^{11} ions/(s × cm^2) level, the high concentration of hydrogen implanted near the copper and titanium surfaces is immobile at room temperature after 10^3 min of continuous irradiation. This implies that when the RANS-II solid lithium target backing material is titanium or copper, neutron generation is performed with an H^+ beam current of 10 μA, and no breakage is caused by hydrogen diffusion between the backing material and the neutron generation layer after about 1 hour of operation.

5. Conclusion

In this study, hydrogen accumulation at shallow areas in the backing materials of the compact accelerator neutron source was reproduced by using a low energy ion implantation system, and the hydrogen distribution spectra of the alternative backing material titanium and current backing material copper were analyzed using the ERDA beam analysis method. The spectra obtained from SRIM and SIMNRA simulations were compared with ERDA analysis experiments, confirming the validity of the peak positions and FWHM of the ERDA experimental spectra. It is confirmed that irradiation of metal samples with a low-energy proton beam can achieve proton concentrations reach several percent at a depth of hundreds of nanometers from the sample surface within a short period and using the ERDA beam analysis technique can analyze the distribution of protons that stop near the surface of the metal sample. These research methods are essential for studying the proton behavior at the junction of the neutron generation film and the backing material during the neutron generation process of the solid neutron generation target, which is of great significance for the

development of long-life solid neutron generation targets for the compact accelerator-neutron source.

Acknowledgements

We thank Yasutaka Morimitsu from the Department of Mechanical Systems Engineering, Tokyo City University, and Dr. Tokihiro Ikeda from the RIKEN Nishina Center for Accelerator-Based Science Detector Team for their support in the sample production and ERDA.

References

[1] M.R. Hawkesworth, *Atomic Energy Review* 152 (1977), p. 169.
[2] T. Kobayashi, S. Ikeda, et al., *Nuclear Instruments and Methods in Physics Research Section* A 994 (2021), 165091.
[3] Y. Yamagata, K. Hirota, et al., *Journal of Radioanalytical and Nuclear Chemistry* 305 (2015), pp. 787-794.
[4] O. Yamada, F. Ono, et al., *Solid State Communications* 42 (1982), pp. 473-475.
[5] I. Uehara, *Journal of the Hydrogen Energy Systems Society of Japan* 25 (2000), p.2.
[6] F.W. Wiffen, and R.T. Santoro, *Proceedings of the Topical Conference on Ferritic Alloys for use in Nuclear Energy Technologies* (1983), p.195, Snowbird, USA.
[7] D. Cao, L. Wu, et al., *Journal of Power Sources* 177 (2008), pp. 624-630.
[8] A.S. Dalton, A.A. Belak, et al., *Chemistry of Materials* 24 (2012), pp. 1568-1574.
[9] H.-F. Liu, N. Hagura, et al., *Journal of Physics.: Conference Series* 2326 (2022), 012018.
[10] M. Noriaki. *Applied Physics* 54 (1985), pp.471-477.
[11] M. Mayer, *American Institute of Physics Conference Proceedings* 475 (1999), p. 541.